

Persistence of exon 2 skipping and dystrophin expression at 18 months after U7snRNA-mediated therapy in the Dup2 mouse model

Liubov V. Gushchina,^{1,2,4} Adrienne J. Bradley,^{1,4} Tatyana A. Vetter,^{1,2} Jacob W. Lay,¹ Natalie L. Rohan,¹ Emma C. Frair,¹ Nicolas Wein,^{1,2} and Kevin M. Flanigan^{1,2,3}

¹The Center for Gene Therapy, Nationwide Children's Hospital and The Ohio State University, Columbus, OH, USA; ²Department of Pediatrics, The Ohio State University, Columbus, OH, USA; ³Department of Neurology, The Ohio State University, Columbus, OH, USA

Duchenne muscular dystrophy (DMD) is a progressive X-linked disease caused by mutations in the DMD gene that prevent the expression of a functional dystrophin protein. Exon duplications represent 6%–11% of mutations, and duplications of exon 2 (Dup2) are the most common (~11%) of duplication mutations. An exon-skipping strategy for Dup2 mutations presents a large therapeutic window. Skipping one exon copy results in full-length dystrophin expression, whereas skipping of both copies (Del2) activates an internal ribosomal entry site (IRES) in exon 5, inducing the expression of a highly functional truncated dystrophin isoform. We have previously confirmed the therapeutic efficacy of AAV9.U7snRNA-mediated skipping in the Dup2 mouse model and showed the absence of off-target splicing effects and lack of toxicity in mice and nonhuman primates. Here, we report long-term dystrophin expression data following the treatment of 3-month-old Dup2 mice with the scAAV9.U7.ACCA vector. Significant exon 2 skipping and robust dystrophin expression in the muscles and hearts of treated mice persist at 18 months after treatment, along with the partial rescue of muscle function. These data extend our previous findings and show that scAAV9.U7.ACCA provides long-term protection by restoring the disrupted dystrophin reading frame in the context of exon 2 duplications.

INTRODUCTION

Duchenne muscular dystrophy (DMD) is a severe muscle disorder that results in worsening muscle weakness and affects ~1:5000 male births.¹ DMD is caused by mutations that affect the reading frame of the *DMD* gene, resulting in the loss of functional dystrophin protein. Although most mutations consist of deletions of one or more exons, exon duplications account for between 6% and 11% of all mutations.^{2,3} Among these, duplications of exon 2 are most prevalent, accounting for ~11% of all duplications.⁴

Single-exon duplications present a promising target for exon-skipping therapies. US Food and Drug Administration–approved exon-skipping therapies (including the phosphorodiamidite morpholino oligomers [PMOs] eteplirsen, golodirsen, casimesen, and viltolarsen)

are commonly used in patients with exon deletions; by skipping an exon flanking a deletion, they result in the restoration of the reading frame and expression of an internally deleted but partially functional dystrophin.^{5–8} In contrast, skipping one copy of a duplicated exon restores an entirely normal mRNA, resulting in the expression of full-length dystrophin protein. Exon 2 duplications are a particularly promising target, as “overskipping,” or excision of both exon 2 copies, results in the use of an internal ribosome entry site (IRES) found in exon 5.⁹ The protein product of IRES-driven expression is an N-terminal-deleted yet highly functional dystrophin protein compatible with ambulation into the seventh or eighth decade.^{10,11}

We have developed an approach to viral vector-mediated exon skipping using an adeno-associated viral (AAV) 9 vector with 4 copies of U7snRNA targeting the exon 2 splice acceptor and splice donor sites.⁹ This vector, scAAV9.U7.ACCA, has been shown to restore dystrophin mRNA and protein expression in a dose-dependent manner,¹² without evidence of off-target splicing effects¹³ or toxicity¹⁴ at clinically relevant dosages. These results led to the approval of a first-in-human trial that is under way ([Clinicaltrials.gov NCT04240314](https://clinicaltrials.gov/ct2/show/study/NCT04240314)).

Here, we report the long-term efficacy of the scAAV9.U7.ACCA vector in 3-month-old Dup2 mice as assessed at 18 months postinjection. A single systemic injection at the minimally efficacious dose (MED) of 3×10^{13} vg/kg results in significant exon 2 skipping and robust dystrophin expression in skeletal muscles, diaphragms (Dias), and hearts of treated mice, along with the partial rescue of muscle function in both tibialis anterior (TA) and Dia and better protection of the TA muscle from repeated fatigue. The biodistribution confirms the long-term vector transduction in skeletal muscles and organs 18 months postvector administration. Together, these data define the long-term efficacy of

Received 22 August 2023; accepted 24 October 2023;
<https://doi.org/10.1016/j.omtm.2023.101144>

⁴These authors contributed equally

Correspondence: Kevin M. Flanigan, The Center for Gene Therapy, Nationwide Children's Hospital, Columbus, OH, USA.

E-mail: kevin.flanigan@nationwidechildrens.org



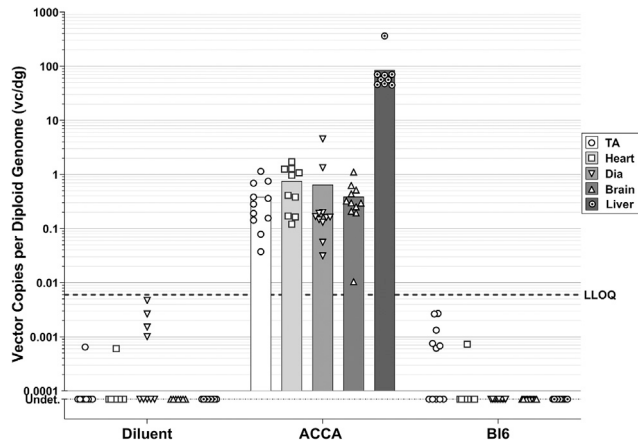


Figure 1. TaqMan qPCR quantification of scAAV9.U7.ACCA vector genome biodistribution

AAV9 vector copy (vc) per diploid genome (dg) in TA, heart, Dia, brain, and liver from untreated Bl6 ($n = 10-11$), Dup2-diluent (Diluent) ($n = 7-9$) or Dup2-ACCA (ACCA) ($n = 10-11$) mice. Data are presented as mean with individual points. LLOQ, lower limit of quantification; Undet., undetermined.

scAAV9.U7.ACCA, suggesting it as a therapy for the treatment of DMD patients with exon 2 duplications.

RESULTS

Clinical and anatomical pathology findings

Three groups of male mice were evaluated in the study and sacrificed at 19–21 months of age: (1) Dup2 mice treated at age 3 months with scAAV9.U7.ACCA (Dup2-ACCA) at the expected MED¹² of 3×10^{13} vg/kg ($n = 11$), (2) Dup2 mice treated at age 3 months with diluent ($n = 11$) (Dup2-diluent), and (3) C57Bl/6 (Bl6) untreated mice ($n = 11$). All Dup2-ACCA- and Dup2-diluent-treated animals tolerated dosing and showed no clinical findings that suggested toxicity throughout the period of the study. Two of 11 Dup2 mice with treated with diluent alone died at 78 weeks of age, or 66 weeks after diluent injection. All of the mice injected with scAAV9.U7.ACCA survived to the predefined endpoint of 18 months. However, at the time of necropsy, one Dup2-ACCA-treated mouse was found to have an enlarged spleen and a second Dup2-diluent-treated mouse was found to have a fluid-filled liver mass. Limited histopathology was completed, with no significant findings. Bl6 males were received from The Jackson Laboratory (Bar Harbor, ME) at 17 months of age and were sacrificed 2 months later. Animal weights at necropsy for each group are included in Table S1. There were no significant differences in body weights between groups.

Vector biodistribution

Biodistribution of the transgene was assessed by qPCR in the TA, Dia, heart, brain, and liver (Table S2). Consistent with known AAV9 tropism, the highest number of vector copies per diploid genome (vc/dg) was seen in the liver (85.47 ± 27.91 vc/dg). Dia and heart had similar amounts of the AAV genome ranging from 0.65 ± 0.40

to 0.75 ± 0.18 vc/dg. TA and brain tissues also showed similar amounts ($0.38-0.39$ vc/dg) of vector (Figure 1). All of the control samples from untreated Bl6 and Dup2-diluent mice had undetectable levels or levels below the lower limit of quantification (LLOQ; 0.006 vc/dg).

RT-PCR Dmd exon 2 skipping

We have previously shown that following the systemic delivery of scAAV9.U7.ACCA in Dup2 mice, three transcripts are possible: one carrying a duplicated exon 2 (Dup2), a wild-type (WT) transcript with a single copy of exon 2, and a Del2 transcript that contains no copies of exon 2.^{12,15} Both WT and Del2 are considered therapeutic since the Del2 results in the activation of the exon 5 IRES.⁹ As expected, Bl6 mice showed only the WT transcript, whereas Dup2-diluent mice demonstrated a very low level of exon 2 exclusion, with an average of $3.19\% \pm 1.03\%$ of detectable transcript being WT transcript in the TA muscle, which is consistent with our previous observations (Figures 2A and 2B; Table S3). The administration of scAAV9.U7.ACCA resulted in significant skipping of exon 2, with mean therapeutic transcript levels of $45.98\% \pm 6.7\%$ in TA, $73.44\% \pm 5.17\%$ in heart, and $31.82\% \pm 4.71\%$ in Dia of treated mice (Figure 2C).

Dystrophin protein expression

Immunofluorescent staining showed a substantial increase in the percentage of dystrophin-positive fibers (PDPFs) in Dup2-ACCA mice compared to Dup2-diluent mice (Figure 3A). Hearts showed the greatest increase after treatment, with the mean PDPFs increasing from $1.18\% \pm 0.19\%$ in Dup2-diluent mice to $96.5\% \pm 0.68\%$ in Dup2-ACCA mice. TA muscle showed a PDPF increase from $12.47\% \pm 1.67\%$ to $51.87\% \pm 7.15\%$, and Dia showed an increase from $4.03\% \pm 1.21\%$ to $47.45\% \pm 2.87\%$ after scAAV9.U7.ACCA treatment. As expected, Bl6 mice had $\geq 96\%$ PDPFs, with the mean PDPFs ranging from $96.33\% \pm 0.91\%$ in Dia to $99.90\% \pm 0.04\%$ in heart (Figure 3B; Table S4).

Dystrophin fluorescence intensity measured at the sarcolemma in all of the tissues further confirmed the efficacy of scAAV9.U7.ACCA treatment. The heart displayed the greatest dystrophin intensity, with an average value reaching $43.13\% \pm 1.7\%$ of Bl6 mean dystrophin intensity. In both TA and Dia tissues from Dup2-ACCA mice, the mean dystrophin intensity also changed significantly, reaching $25.66\%-29.59\%$ of Bl6 mean dystrophin intensity (Figures 3A, 3C, and S1; Table S4).

Western blot (WB) analysis was performed to quantify the total amount of protein expression using a 5-point standard curve (0%–80%) of pooled Bl6 tissues and a C-terminal dystrophin antibody that recognizes both full-length and IRES-driven dystrophin protein isoforms. Dup2-diluent mice showed low to moderate levels of dystrophin, ranging from 3.01% to 13.4% in the tested tissues (Table S5), which is consistent with our previous publications using this model.^{9,12,16,17} In Dup2-ACCA mice, persistent restoration of dystrophin was observed in all of the tissues tested. Consistent with

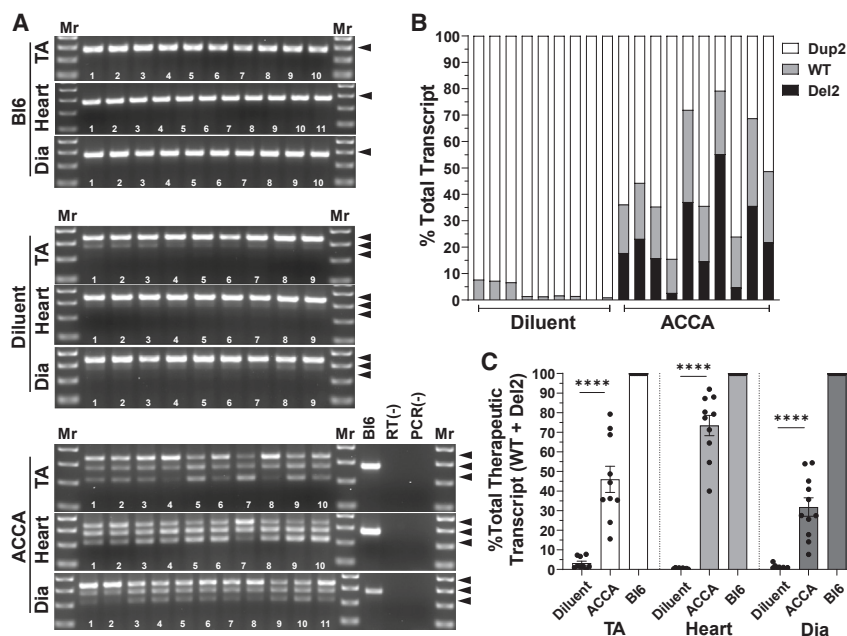


Figure 2. *Dmd* exon 2 skipping in Dup2 mice systemically administered with scAAV9.U7.ACCA

(A) RT-PCR gel images of TA, heart, and Dia RNA from Dup2-ACCA (ACCA) receiving the dose of 3×10^{13} vg/kg 18 months postinjection, compared to Dup2-diluent (Diluent) and untreated Bl6 control mice. Black arrows display up to 3 amplicons containing either 2 copies (Dup2, 340 bp), 1 copy (WT, 278 bp), or no copies (Del2, 216 bp) of exon 2. (B) Quantification of RT-PCR amplicon bands (shown in A) is represented as percentage of total *Dmd* transcript in the right side of TA muscle in individual animals. Dup2 band is shown in white, whereas skipped transcripts, defined as WT and Del2 dystrophin transcripts, are shown in gray and black, respectively. All Bl6 mice show exclusively WT transcript and were not included in the figure. (C) RT-PCR quantification analysis in TA, heart and Dia tissues. Data presented as mean \pm SEM ($n = 9-11$) with individual points. Statistical comparisons performed using unpaired t test. Groups without variation—all Bl6—were excluded from statistical analysis. Statistical comparison markers indicate which groups were analyzed: **** $p < 0.0001$.

RT-PCR and immunofluorescence (IF) results, WB analysis also revealed the highest level of dystrophin observed in the heart, reaching $65.36\% \pm 5.12\%$ of WT protein 18 months post-scAAV9.U7.ACCA injection (Figures 4 and S2). An average of $41.92\% \pm 8.93\%$ and $17.68\% \pm 1.89\%$ of WT dystrophin was detected in TA and Dia, respectively (Table S5).

Muscle function assessments

To examine whether the dystrophin restoration leads to a sustained recovery of muscle strength in Dup2 mice 18 months post-scAAV9.U7.ACCA treatment, *in situ* (TA) and *in vitro* (Dia) muscle function assessments were performed. Tetanic-specific force in both TA and Dia and force retained following a cycle of eccentric contractions (ECCs) of the TA muscle were measured (Figure 5). Dup2-diluent mice exhibited marked functional deficits compared with Bl6 control mice, with 38.4% less tetanic force output in TA (147.7 ± 4.23 mN/mm² versus 239.8 ± 10.78 mN/mm²) and 50.2% less tetanic force output in Dia (123.0 ± 9.25 mN/mm² versus 246.9 ± 18.99 mN/mm²) (Figure 5A). Moreover, these Dup2-diluent mice also displayed a greater loss of force following repetitive ECCs compared with Bl6 mice (74.3% loss in Dup2-diluent versus 12.6% loss in Bl6 mice). The area under the curve (AUC) of the ECC tracings confirmed this observation, showing a Dup2-diluent AUC up to 50.6% of Bl6 (Figures 5B and 5C). Systemic administration of scAAV9.U7.ACCA resulted in an increase in force output in the TA and Dia tissues, reaching 70.1%–73.3% of Bl6 muscles. Significant rescue of ECC-induced force loss was also observed in the TA muscle after scAAV9.U7.ACCA injection (46.76% loss in Dup2-ACCA versus 12.54% loss in Bl6 mice), with AUC values reaching 72.9% of Bl6 muscle (619 ± 40.75 in Dup2-ACCA versus 848.6 ± 17.76 in Bl6 mice) (Figure 5; Table S6).

Long-term histological and morphological effects

To demonstrate the long-term benefit of intravenously administered scAAV9.U7.ACCA vector in Dup2 mice, animals were evaluated for histopathological and morphometric changes 18 months after vector treatment (Figure 6). Analysis revealed significant more centrally nucleated fibers (CNFs) in both TA and Dia tissues in both Dup2-diluent and Dup2-ACCA mice compared with Bl6 controls. A relatively small but significant increase in the percentage of CNFs was also observed in scAAV9.U7.ACCA-treated TA but not Dia muscles compared with Dup2-diluent-treated mice (Figures 6 and S3; Table S7). In addition, scAAV9.U7.ACCA treatment resulted in partial normalization of the mean myofiber diameter distribution in the TA (43.72 ± 0.74 μ m in Dup2-diluent versus 47.71 ± 0.94 μ m in Dup2-ACCA groups) and Dia (25.50 ± 0.46 μ m in Dup2-diluent versus 28.60 ± 0.32 μ m in Dup2-ACCA groups) muscles (Figure 6C; Table S7).

DISCUSSION

Vectorized exon skipping using U7snRNA is potentially advantageous over antisense oligonucleotide therapies because of the high efficiency of skipping that can be achieved and because the long-lasting effects of a single injection may obviate the need for weekly or monthly injections over a patient's lifetime. Our previous studies in Dup2 mice treated with various doses of the scAAV9.U7.ACCA vector established the MED of 3×10^{13} vg/kg¹² and demonstrated significant dystrophin expression and improvement in force generation defects in muscle up to 6 months after treatment at doses ranging from 7.6×10^{13} vg/kg to 3.2×10^{14} vg/kg¹⁵.

The present study extends those prior results, providing evidence for durability by demonstrating prolonged effects on exon 2

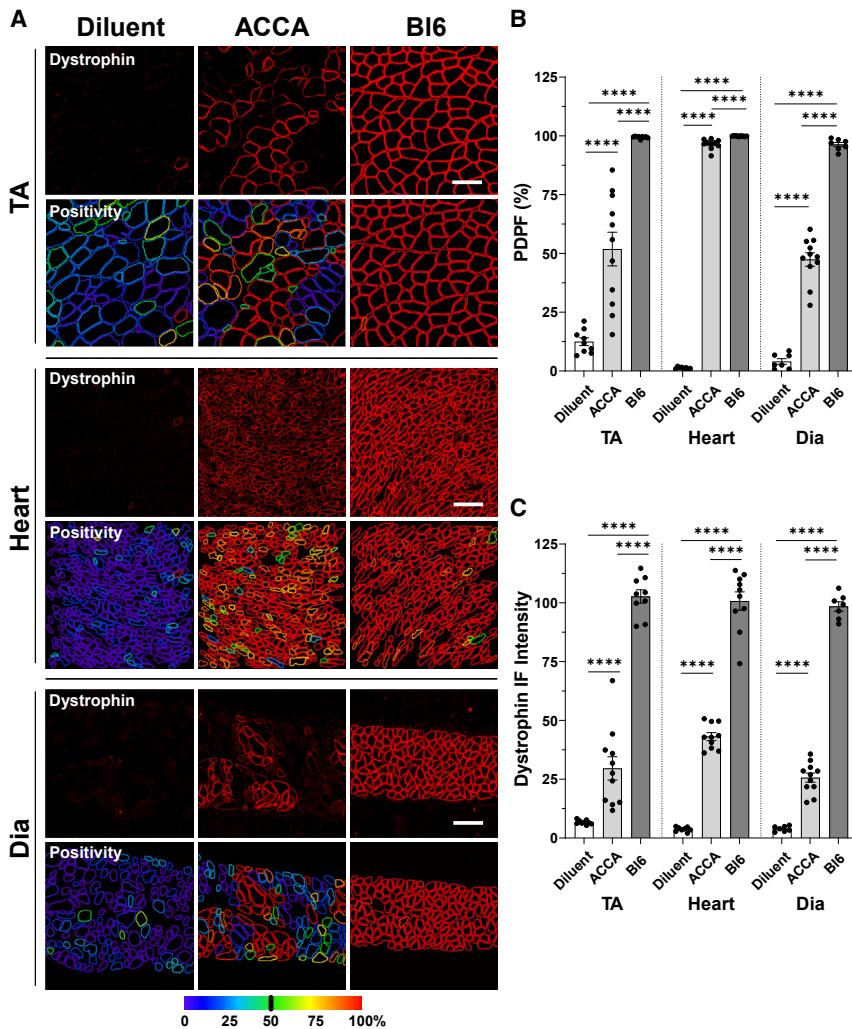


Figure 3. Dystrophin expression in skeletal muscles and heart 18 months post-scAAV9.U7.ACCA administration

Representative immunofluorescent images show selected ROIs of (A) left TA, heart, and Dia sections with dystrophin in red displaying localization and intensity of dystrophin signal in BI6, Dup2-diluent (Diluent), or Dup2-ACCA (ACCA) mice. Color-coded heatmaps of each tissue demonstrate the percentage of the perimeter with dystrophin-positive pixels (positivity) for each muscle fiber. Fibers with $\geq 50\%$ dystrophin-positive perimeter are considered overall positive for dystrophin. Scale bars represent 100 μm . Color key in bottom left corner shows color to percentage conversion for dystrophin-positive perimeter. Quantification analysis of images from (A) showing the PDPFs (B) and dystrophin intensities (C) in TA, heart, and Dia tissues. Data are presented as mean \pm SEM, with individual points. Statistical comparisons were performed using 1-way ANOVA with Sidak's multiple comparisons test; **** $p < 0.0001$. See also Figure S1 for color-coded heatmaps of normalized dystrophin intensity.

ous publications demonstrating similar levels of dystrophin in the Dup2 mouse model.^{12,15–17}

Consistent with the WB results, IF analysis confirms long-term dystrophin expression and its proper localization at the sarcolemmal membrane at levels that can be expected to prevent disease progression and provide therapeutic benefits to patients with DMD. The persistence of long-term dystrophin expression in the heart is of particular clinical importance because cardiomyopathy is a leading cause of death in patients with DMD.¹⁹ Notably, the level of full-length and IRES-driven dystrophin isoforms that we observe in Dup2 mice at 18 months post-scAAV9.U7.ACCA administration has not been reached in animal studies of microdystrophin, other U7snRNA vectors, or morpholino oligomers (~ 6 –12 months).^{20–23}

We note that expression was somewhat diminished in comparison to our shorter-term studies, with an approximately 2- to 2.5-fold reduction in the amount of exon 2 exclusion in TA and Dia in comparison to either 3- or 6-month studies.^{12,15} In contrast, exon 2 exclusion remains comparable in the heart regardless of the dose administered or the age at treatment, showing only a slight decrease ($\sim 6\%$ – 19%) in this 18-month study. Although these data may be consistent with a decline in efficacy over time, an alternate explanation is that vector administration at a younger age may be more efficacious, a hypothesis potentially supported by the result of our first in-human trial (NCT04240314) in three participants, in whom the most robust expression was clearly found in the participant treated in infancy (7 months) as opposed to late childhood.²⁴

exclusion and on dystrophin expression in both skeletal muscles and heart 18 months following delivery to adult mice. Significant levels of dystrophin protein were achieved and maintained at 18 months postinjection, suggesting that treatment with scAAV9.U7.ACCA results in the translation of a stable dystrophin protein. Although use of a C-terminal antibody cannot reliably distinguish between the full-length WT (427 kDa) and the IRES-driven (413 kDa) proteins under WB conditions for which technical replicate reproducibility has been established, we note that in the clinical setting, the expression of only 15% of normal of the IRES-driven isoform alone is sufficient to allow ambulation into at least the seventh decade.¹¹ Either some baseline utilization of the IRES (even in the Dup2 context) or some low-level baseline exclusion of a single exon 2 copy may account for some of the observed variability among Dup2 patients; 70% have a typical DMD phenotype, whereas the other 30% are characterized as milder dystrophinopathies.¹⁸ These hypotheses are supported by the relatively high level of dystrophin protein expression (up to $\sim 13.4\%$) detected by WB in the TA muscle of Dup2 mice treated with diluent, which is consistent with our previ-

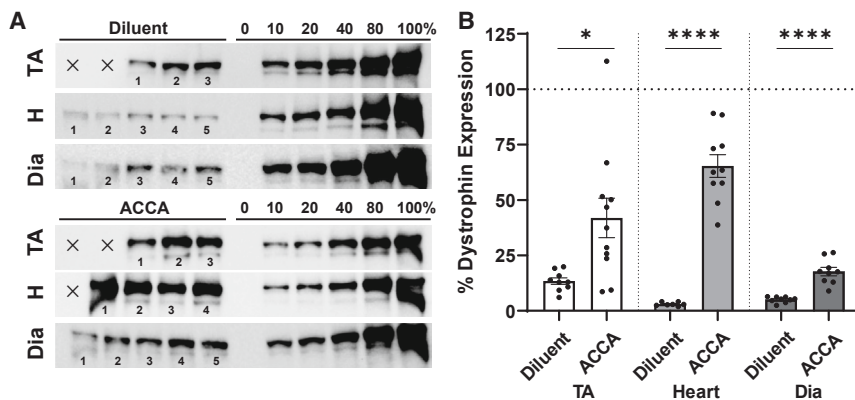


Figure 4. Long-term restoration of full-length dystrophin in Dup2 mice following systemically administered ACCA 18 months postinjection

(A) Representative WB images of left TA muscles, heart (H), and Dia (1 blot per group per tissue) showing dystrophin expression in Dup2 mice treated with diluent (Diluent) or scAAV9.U7.ACCA (ACCA) vector 18 months postinjection. Individual samples are numbered 1–5, and the right 6 lanes of every blot contain a 6-point standard curve of pooled Bl6 ($n = 7–8$) lysate diluted in Dup2Del18-41 dystrophin-null muscle lysate, ranging from 0% to 100%. (B) Normalized dystrophin levels in Dup2-diluent or Dup2-ACCA mice. For protein quantification, a 5-point Bl6 standard curve (0%–80%) with $R^2 \geq 0.9753$ was accepted for data analysis. The dashed line indicates 100% based on the pooled Bl6 standard curve. Data

presented as mean \pm SEM ($n = 7–11$) with individual points. Statistical comparisons performed using unpaired t test: * $p < 0.05$; **** $p < 0.0001$. See also Figure S2, which shows the original WB images for all tissues and dystrophin quantification analysis.

The consistently high long-term expression dystrophin observed in this study also resulted in a significant improvement in muscle function in both TA and Dia muscles compared to Dup2 diluent-treated mice. Previous studies have demonstrated that $2 \times -10 \times$ MED scAAV9.U7.ACCA injection into P0/P1 neonatal or adult Dup2 mice resulted in significantly higher specific force during tetanic contraction and a decrease in force drop in ECC studies, as compared to the control Dup2 in the TA muscle 3 or 6 months after vector administration.^{12,15} In contrast, the results presented here at 18 months after scAAV9.U7.ACCA injection demonstrate a greater reduction in TA ECC force drop (to 53.2% of Bl6 in the present study) versus that observed at 3 or 6 months following P0/P1 injection or at 3 months following the injection of 2-month-old mice (63%–78% ECC drop and $\sim 10\%$ –22% AUC),¹⁵ consistent with the drop in dystrophin expression over the same period. The observation in the Dup2-ACCA group of a significant increase in CNFs at 18 months is unexpected because it contrasts with what was previously seen at shorter posttreatment intervals with both scAAV9.U7.ACCA and peptide-linked phosphorodiamidate morpholino oligomers (PPMO).^{15,17} The reason for this discrepancy is not clear, although a diminished effect on the reduction of central nuclei has been reported in older *mdx* mice treated with a microdystrophin compared to those treated at a younger time point,²⁵ suggesting that age at treatment may play a role in this effect. We note that we delivered the vector to mice aged 3 months, by which time their muscle has gone through a period of degeneration analogous to that observed in the standard *mdx* model, as we noted in our original paper characterizing the Dup2 mouse model.¹⁶ Because central nucleation tends to persist in mice after the resolution of muscle injury (unlike that in humans), the observation of increased CNF in treated mice raises the possibility that muscle fibers are overall better preserved by the expression of low levels of dystrophin, preserving this evidence of the original period of remodeling. We do not believe that this observation is of significant biological relevance, given the correction in function as assessed by electrophysiology.

Long-term expression has been demonstrated in an animal model with microdystrophin.^{26,27} Expression of a full-length dystrophin

may reasonably be expected to confer greater therapeutic benefit than that of microdystrophins, which themselves show significant therapeutic promise.^{27,28} Although AAV delivery at present is considered a one-time treatment due to the immune response,^{29–33} our results suggest that a one-time injection could lead to long-term dystrophin restoration without the need for a second injection, and in a clinical setting, subsequent treatment with alternate exon skipping agents may be possible.¹⁷

Although the cognitive behavioral phenotype has not been assessed in the Dup2 mouse model, the similar levels of vector genomes found in both brain and TA suggest that the scAAV9.U7.ACCA vector may correct dystrophin in the central nervous system. Future studies will address this possibility.

MATERIALS AND METHODS

scAAV9.U7.ACCA vector production

The scAAV9.U7.ACCA vector for this study was produced at the vector core of the Abigail Wexner Research Institute (AWRI) at Nationwide Children's Hospital (NCH) under research-grade, non-Good Laboratory Practices conditions. The physical titer of the vector was determined by qPCR according to a linearized plasmid standard.

Animal studies

Dup2 male mice¹⁶ were housed in standardized conditions at the NCH animal facility, provided normal chow, water *ad libitum*, and maintained under 12:12-h light:dark cycles. The C57Bl/6 (Bl6) mice were purchased from The Jackson Laboratory (stock no. 000664), acclimatized for 2 months in the vivarium before necropsy, and used as age-matched study controls. All of the animal studies were performed according to the guidelines and approval of the Institutional Animal Care and Use Committee (IACUC) of the AWRI, NCH (IACUC protocol no. AR10-0002 and Institutional Biological and Chemical Safety Committee protocol no. IBS00000370).

scAAV9.U7.ACCA vector was systemically delivered to Dup2 mice aged 11–12 weeks via the tail vein at a dose of 3×10^{13} vg/kg in

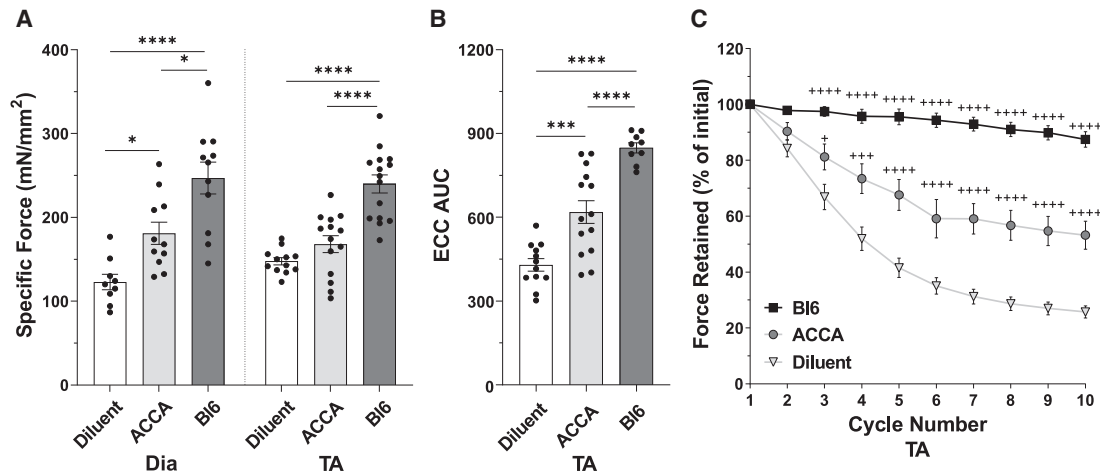


Figure 5. Sustained long-term functional muscle correction following systemic administration of scAAV9.U7.ACCA

(A) Specific force measured for diaphragm ($n = 9-11$) and TA ($n = 9-11$, both legs analyzed independently [$N = 12-15$]) muscles during tetanic contraction in untreated Bl6 mice and Dup2 mice injected with either diluent (Diluent) or scAAV9.U7.ACCA (ACCA). (B) The AUC of ECCs represented in (C) as amplitude of TA force drop over 10 cycles. (C) TA muscle resistance to contraction-induced damage during 10 ECC cycles ($n = 9-11$; both legs analyzed independently [$N = 9-14$]). Data presented as mean \pm SEM, with individual points. Specific force and AUC ECC data were analyzed by 1-way ANOVA followed by Sidak's post hoc analysis for multiple comparisons. * $p < 0.05$; *** $p < 0.001$; **** $p < 0.0001$. Statistical comparison of ECC data was completed using 2-way ANOVA followed by Sidak's post hoc analysis for multiple comparisons. + $p < 0.05$; +++ $p < 0.001$; ++++ $p < 0.0001$ versus Dup2.

lactated Ringer's solution (LRS) in a 200- μ L total volume. Age-matched Dup2 males treated with diluent, containing LRS with 0.01% Poloxamer 188 in the same volume, and untreated Bl6 males were used as controls. Mice were sacrificed 88-91 weeks (18 months) after vector or diluent administration using a lethal dose of ketamine/xylazine (KX) cocktail (NCH Pharmacy). Skeletal muscles, heart tissues, and Dia tissues were snap-frozen in liquid nitrogen-cooled isopentane; brain and liver samples were snap-frozen in liquid nitrogen, and then all of the samples were stored at -80°C until use.

RNA extraction and exon 2 skipping quantification analysis

The RNA extraction and RT-PCR analyses of *Dmd* exon 2 skipping were performed as previously described.¹⁷ Briefly, RNA was extracted from all of the frozen tissues through TRIzol/chloroform extraction (Life Technologies, Carlsbad, CA, catalog no. 15596018; Fisher Bio-reagents, Hampton, NH, catalog no. C297-4) and then purified using the RNA Clean & Concentrator-25 kit according to the manufacturer's instruction (Zymo Research, Tustin, CA, catalog no. R1018). The RNA (1 μ g) was converted to cDNA using the RevertAid Reverse transcription kit and random hexamer primers according to the manufacturer's protocol (Thermo Scientific, Waltham, MA, catalog no. K1691). cDNA was amplified via PCR (Thermo Fisher, Waltham, MA, catalog no. K0171) using a set of primers specific to the *Dmd* 5' UTR and the exon 3-4 junction. The amplicons were visualized by gel electrophoresis and images were captured using the ChemiDoc MP imaging system (BioRad, Hercules, CA). Digital images of gels were quantified using ImageJ software (version 1.46r, NIH, Bethesda, MD) to determine the relative amounts of different amplicons. Primer sequences (IDT, Coralville, IA) and the PCR program are available upon request.

TA tetanic and ECC measurements and data analysis

In situ TA muscle contraction assays were conducted using a standard protocol^{34,35} with several modifications, as described previously.¹² Briefly, mice were anesthetized with a KX mixture. The TA muscle was exposed and cleaned from connective tissues, a double square knot was tied to the distal TA tendon with a 3-0 suture (MedPlus Services USA Look, Nashville, TN, catalog no. SP117), and the tendon was cut. The mouse was transferred to a thermally controlled platform and maintained at 37°C (Aurora Scientific, Aurora, ON, Canada). To avoid the drying of tissues, the muscle was constantly dampened with 0.9% sodium chloride solution (saline) during the procedure. The muscle was warmed up using two electrical probes, which were placed in the biceps femoris muscle near the sciatic nerve for stimulation; then, the muscle was stimulated to determine the optimal length (L_0 , mm) and tension to be used throughout the protocol. The active tetanic muscle force was recorded to calculate the absolute force using the Lab View-based DMC program (Aurora Scientific, version 5.200), which was also used for specific force analysis. Following a 5- to 10-min rest, the muscle was subjected to a series of 10 isometric contractions with a 10% stretched length, with 60-s intervals between the stimuli to determine the force drop. For TA-specific force analysis, the muscles were removed and weighed, and the cross-sectional area (CSA) was calculated as follows:

$$\text{CSA}(\text{mm}^2) = \frac{\text{mass}(\text{g})}{(\text{g}/\text{mm}^3) \times R \times L_0(\text{mm})}, \quad (\text{Equation 1})$$

where muscle density (ρ) is $0.00106 \text{ g}/\text{mm}^3$ (or $1.06 \text{ mg}/\text{mm}^3$), R is the ratio of fiber length in the TA, which equals 0.6,³⁶ and L_0 is the muscle length (mm). The CSA and absolute force measurement were used to determine the specific force measurement.

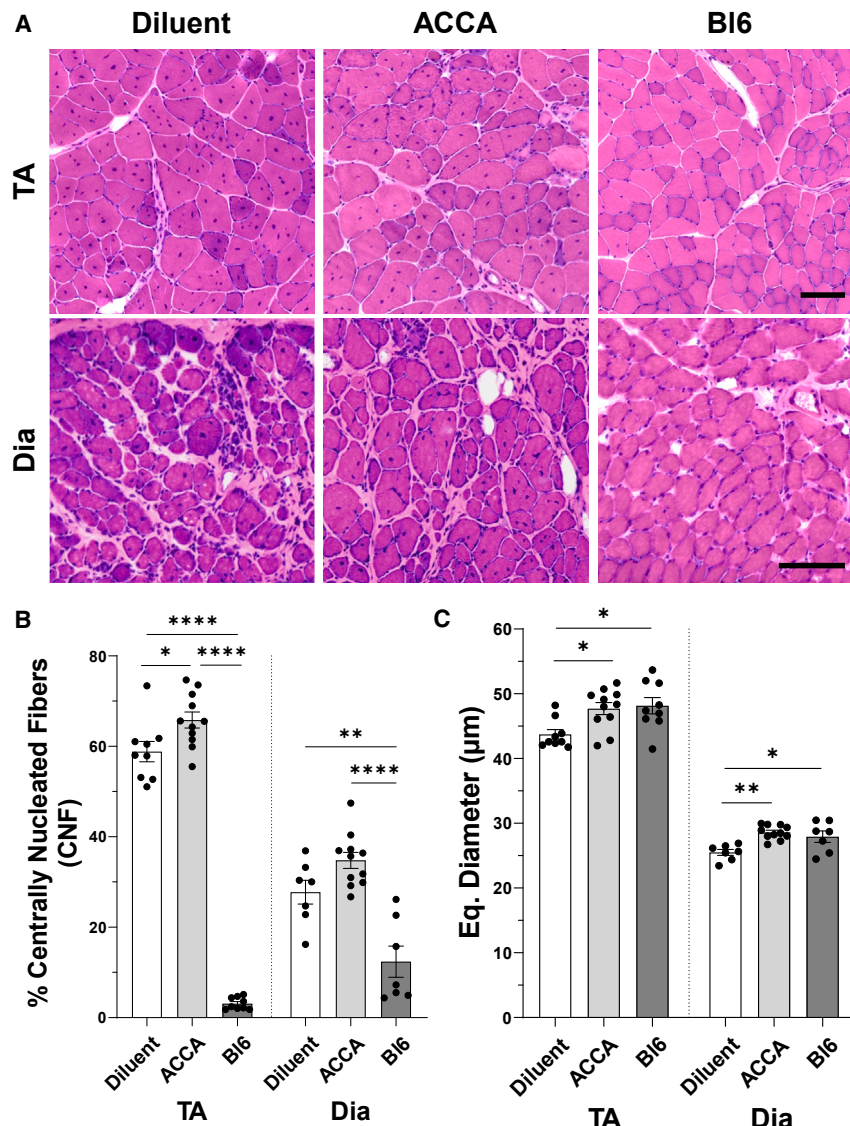


Figure 6. Histological and morphometric analysis of TA and Dia tissues

(A) H&E Y staining of TA and Dia muscles from C57Bl/6 (Bl6), Dup2-diluent (Diluent), or Dup2-ACCA (ACCA). Scale bar represents 100 μm . (B) Quantification analysis of (B) CNFs and (C) equivalent diameter (Eq. Diameter) of the fiber in TA and Dia muscles. Data presented as mean \pm SEM, with individual points. Statistical comparisons were performed using 1-way ANOVA with Sidak's multiple comparisons test; * $p < 0.05$, ** $p < 0.01$, **** $p < 0.0001$. See also Figure S3, which shows representative IF images used for CNFs and equivalent diameter quantification analysis.

in the organ bath to flank the length of the muscle, and then muscle tetanic force was recorded to further determine the absolute and specific tetanic forces. To calculate the specific force in Dia, CSA was determined using Equation 1, in which the ratio of fiber length in the Dia, $R = 1.0$.³⁶

DNA extraction and qPCR vector biodistribution quantification

Genomic DNA extraction and qPCR procedures were performed as previously described.¹⁵ Briefly, total DNA was extracted from all of the tested tissue samples using the DNeasy Blood & Tissue Kit (Qiagen, Germantown, MD, catalog no. 69506), and AAV vector genomes were quantified by qPCR using a linearized pAAV.U7.ACCA plasmid to generate a standard curve for absolute transgene quantification. PCR was performed using TaqMan Universal PCR Master Mix (Applied Biosystems, Foster City, CA, catalog no. 4304437) and Quantstudio6 Flex (Applied Biosystems) following the procedures recommended by the manufacturer and a set of primers unique to the transgene (sequences available upon request). Genomic DNA from untreated Bl6 and diluent-injected Dup2 mouse tissues served as experimental controls. Each sample was run in triplicate. Acceptance criteria for an assay included a standard curve with an $R^2 \geq 0.9900$ or higher, efficiency between 91.4% and 99.7% or a slope between -3.33 and -3.55 , and undetermined values in the nontemplate control reactions.

Absolute vector copies in a reaction were determined based on the transgene specific standard curve and normalized to the total genomic DNA in a given reaction measured by nanodrop spectrophotometer. The amount of vc/dg was calculated based on the assumption of average mouse diploid genome weighing 6 pg (166.67 genomes per nanogram).³⁸ Samples with the positive presence of transgene had values exceeding the lowest detectable point

Dia tetanic contraction measurements and data analysis

In vitro Dia muscle contraction assays were conducted using a standard protocol.³⁷ Briefly, after euthanasia, using a lethal dose of KX mixture, the intact Dia was collected with rib attachments and central tendon and placed in Krebs-Henseleit (K-H) buffer containing 137 mM NaCl, 5 mM KCl, 1.2 mM MgSO_4 , 1.2 mM NaH_2PO_4 , 0.25 mM CaCl_2 , 20 mM NaHCO_3 , 10 mM D-glucose (dextrose), and 20 mM 2,3-butanedione monoxime. Dia strips (2–4 mm wide) were isolated from each mouse. They were tied firmly with a 3-0 suture (MedPlus Services USA Look, catalog no. SP117) at the central tendon and sutured through a portion of rib bone affixed to the distal end of each strip. Each muscle strip was transferred to a thermally controlled water bath (37°C) (Aurora Scientific) filled with oxygenated K-H solution (5% CO_2 balance oxygen). The Dia muscle was warmed up using two platinum plate electrodes that were positioned

on the standard curve, 0.006 vc/dg. The samples that did not pass the threshold by the end of the 40 cycles were reported as undetermined and those below 0.006 vc/dg were considered below the LLOQ and reported as negative. If one of the three replicates in the assay was determined as having a specific copy number, then this sample was reported as the mean with no standard deviation. If two of the three replicates were determined, then the mean and standard deviation for this sample was calculated from the two replicates that generated a value. If all three replicates failed to generate a value, then the mean was reported as undetermined with no standard deviation provided.

IF staining and microscope image analysis

IF staining, imaging, and image analysis were performed as previously described.^{17,39} Briefly, 10- μ m frozen muscle sections were air dried, permeabilized in buffer containing 1 \times PBS with 0.1% Triton X-100 and 10% normal goat serum (NGS) (Invitrogen, Waltham, MA, catalog no. 100000C), and then incubated in blocking buffer containing 1 \times PBS with 0.1% Tween 20 (PBST) and 10% NGS. Sections were then co-stained in a mixture of rabbit monoclonal anti-dystrophin C-terminal antibody (1:400) (Abcam, Cambridge, UK, catalog no. ab218198) and rat anti-laminin antibody (1:400) (R&D Systems, Minneapolis, MN, catalog no. MAB4656) for 2 h at room temperature. Slides were washed 4 times for 5 min in 1 \times PBST; then, they were incubated in a mixture of the appropriate secondary antibodies: donkey anti-rat Alexa Fluor 488 (The Jackson Laboratory, catalog no. 712-546-153) or goat anti-rabbit Alexa Fluor 568 (Invitrogen, catalog no. A-21069) (1:500) for 1 h and washed again 3 times for 5 min. Coverslips were mounted with Prolong Gold with DAPI (Invitrogen, catalog no. P36931).

Whole-section images of TA, Dia, and heart were collected on a fully motorized Nikon Ti2-E inverted microscope with Plan Apochromat Lambda objectives (both Nikon, Tokyo, Japan) and a Hamamatsu (Shizuoka, Japan) ORCA Fusion camera within 24 h of the completion of staining. TA and Dia sections were imaged using 10 \times magnification at a resolution of 0.64 μ m/pixel, and hearts were imaged using 20 \times magnification at a resolution of 0.32 μ m/pixel.

The quantification of muscle dystrophin immunofluorescence was performed in Nikon NIS-Elements AR software using the General Analysis 3 software module and a custom analysis workflow optimized for mouse tissue, as previously described.^{17,39} Muscle fibers with a \geq 50% dystrophin-positive perimeter were considered overall positive and used to calculate the PDPFs for each tissue section. Dystrophin intensity in muscle sections was analyzed by measuring the mean intensity of all of the pixels in the dystrophin channel within a 5- μ m-wide boundary region at the sarcolemma around each muscle fiber.

Heart tissues were analyzed as four-square regions of interest (ROIs) sampled from the transverse myocyte regions of each heart section, with each ROI measuring 0.5 \times 0.5 mm. The same workflow was used to quantify dystrophin-positive myocytes and myocyte dystro-

phin intensity in heart ROIs as the skeletal muscle analysis described above, with the exception of a 3- μ m sarcolemmal boundary. Cardiac myocytes touching the edges of the ROI field were excluded from analysis. Quantification results from the 3 ROIs for each heart were averaged to produce a single result for dystrophin-positive myocytes and myocyte dystrophin intensities for each heart.

Muscle morphometric analysis

Morphometric parameters of muscle fiber size (as equivalent diameter) and the percentage of centralized nuclei were quantified as a part of the dystrophin analysis pathway. In TA and Dia tissues, muscle fibers showing at least one DAPI nucleus overlapping with the interior region of the fiber that was eroded in from the laminin-positive sarcolemma by 5 μ m were identified as CNFs. Each fiber with one or more DAPI-stained central nucleus was considered overall to be a CNF. All of the representative images were selected to appropriately reflect the center of the distribution of the group rather than any extreme values or outliers.

Histochemical staining

H&E Y staining was performed on whole sections of cryosectioned tissue. Tissue was sectioned at 10 μ m and allowed to acclimate before a 6-min incubation in hematoxylin (Thermo Fisher, catalog no. 7211L). Slides were then rinsed in dH₂O and dipped in bluing reagent (Thermo Fisher, catalog no. 7301). Slides were dipped in eosin Y (Thermo Fisher, catalog no. 7111L) and staining proceeded as follows: 30% ethanol (EtOH), 3 \times 95% EtOH, 3 \times 100% EtOH, 2 \times xylenes (Thermo Fisher, catalog no. X3F). Coverslips were affixed using cyto seal 60 (Thermo Fisher, catalog no. 23-244256). Slides were imaged using a motorized Nikon Ti2-E microscope with a 10 \times Plan Apochromat Lambda objective and with a Nikon DS-Ri-2 color camera at a resolution of 0.72 μ m/pixel.

Western blotting

Protein was extracted using a lysis buffer containing 4 M urea, 125 mM Tris-HCl, pH 6.8, 4% SDS, and protein inhibitor cocktail (Sigma Aldrich, St. Louis, MO, catalog no. 11836170001). Briefly, 150 μ L of lysis buffer was added to 10 sections of 20- μ m thick tissue. Tissue was lysed using a metal bead and disrupted for 2 min at 30 Hz (TissueLyser II, Qiagen) followed by a 30-min incubation at room temperature before a second lysis step (1 min at 30 Hz, TissueLyser II, Qiagen). The lysate was centrifuged at 14,000 \times g for 20 min and the supernatant was collected for analysis. The protein concentration was quantified using the BioRad DC assay kit (BioRad, catalog no. 5000112) following the manufacturer's protocol. A calibration curve was made by combining lysates from Bl6 mice (n = 8) and dystrophin-null age-matched Dup2Del18-41 mice (n = 4). These Dup2Del18-41 mice were received due to spontaneous mutation in the Dup2 colony and showed a complete absence of dystrophin protein. The supernatant was mixed with a 4 \times Laemmli sample buffer and heated for 5 min at 95°C. Total protein at 22.5 μ g was run on a precast 3%–8% Tris-Acetate NuPage gel (Invitrogen, catalog no. EA0378BOX) for 1 h at 80 V followed by 2 h at 120 V. Protein was transferred from gels to a 0.45- μ m polyvinylidene fluoride membrane

(BioRad, catalog no. 1620260) at a constant 55-mA current overnight at 4°C. HiMark prestained protein standard (Invitrogen, catalog no. LC5699) and/or Precision Plus Protein Dual Color Standards (BioRad, catalog no. 1610394) were used to determine the size of proteins of interest during separation and transfer. Membranes were probed with a rabbit monoclonal anti-dystrophin C-terminal antibody (Abcam, catalog no. ab154168) at 1:1000 dilution in 5% nonfat dry milk in PBST buffer for 2 h. Blots were then washed for 5 × 5 min with PBST. Membranes were exposed to the secondary antibody, goat anti-rabbit horseradish peroxidase (1:5000) for 1 h at room temperature, followed by 5 × 5-min washes with PBST and a 1 × 5-min wash with PBS. Membranes were incubated with 2 mL of enhanced chemiluminescence reagent (Thermo Scientific, catalog no. 34580) before visualization on a Chemidoc MP Imaging System (BioRad). Dystrophin signals were quantified by densitometric analysis using Image Lab software (BioRad, version 6.0.0, build 25). A linear regression curve fit to the calibration curve on each gel was calculated using the 0%–80% WT dystrophin points, and individual samples were quantified against that curve and presented as percentage of WT dystrophin expression. The acceptance criterion for a given blot was defined as $R^2 \geq 0.90$; for all of the blots included in the analysis, the actual R^2 values were ≥ 0.96 .

Statistical analysis

Statistical analyses were performed using GraphPad Prism (Boston, MA, version 9.0). All of the results are presented as mean value ± SEM with individual points. Experiments with a single independent variable were analyzed using one-way ANOVA with the Sidak's multiple comparisons test or unpaired t test if involving only one comparison. The statistical analysis of ECC-induced force loss was completed using two-way ANOVA followed by Sidak's post hoc analysis for multiple comparisons. All of the statistical methods are identified in the legends for the corresponding figures. Significance was determined based on $\alpha = 0.05$.

DATA AND CODE AVAILABILITY

Qualified researchers may request access to the data that support the findings of this study from the corresponding author by contacting kevin.flanigan@nationwidechildrens.org.

SUPPLEMENTAL INFORMATION

Supplemental information can be found online at <https://doi.org/10.1016/j.omtm.2023.101144>.

ACKNOWLEDGMENTS

The authors acknowledge the technical assistance of Nianyuan Huang, Calli Bellinger, Aisha Suhaiba, and Kelly M. Grounds. We thank Drs. Megan Waldrop and Stefan Nicolau for their thoughtful review of the manuscript. Vector production was supported by the Beauhawks Foundation. This study was supported by the NCH and NIH/National Institute of Arthritis and Musculoskeletal and Skin Diseases Center of Research Translation in Muscular Dystrophy Therapeutic Development (P50AR070604).

AUTHOR CONTRIBUTIONS

L.V.G. designed the study, acquired the data, interpreted the data, created the figures, and drafted the manuscript. A.J.B. developed the WB analysis, acquired the data, interpreted the data, created the figures, and drafted the manuscript. E.C.F. assisted in the study design, and E.C.F., J.L., and N.R. acquired the data, interpreted the data, and created the figures. T.A.V. developed the quantitative image analysis, acquired and interpreted the data, and supported the creation of the figures. N.W. and K.M.F. designed the study, reviewed and interpreted the data, and reviewed the manuscript.

DECLARATION OF INTERESTS

NCH licensed the vector described herein to Audentes Therapeutics, which was subsequently acquired by Astellas Therapeutics. N.W. and K.M.F. have received royalty payments as a result of this license.

REFERENCES

1. Crisafulli, S., Sultana, J., Fontana, A., Salvo, F., Messina, S., and Trifirò, G. (2020). Global epidemiology of Duchenne muscular dystrophy: an updated systematic review and meta-analysis. *Orphanet J. Rare Dis.* 15, 141. <https://doi.org/10.1186/s13023-020-01430-8>.
2. Dent, K.M., Dunn, D.M., von Niederhausern, A.C., Aoyagi, A.T., Kerr, L., Bromberg, M.B., Hart, K.J., Tuohy, T., White, S., den Dunnen, J.T., et al. (2005). Improved molecular diagnosis of dystrophinopathies in an unselected clinical cohort. *Am. J. Med. Genet.* 134, 295–298. <https://doi.org/10.1002/ajmg.a.30617>.
3. Aartsma-Rus, A., Van Deutekom, J.C.T., Fokkema, I.F., Van Ommen, G.J.B., and Den Dunnen, J.T. (2006). Entries in the Leiden Duchenne muscular dystrophy mutation database: an overview of mutation types and paradoxical cases that confirm the reading-frame rule. *Muscle Nerve* 34, 135–144. <https://doi.org/10.1002/mus.20586>.
4. White, S.J., Aartsma-Rus, A., Flanigan, K.M., Weiss, R.B., Kneppers, A.L.J., Lalic, T., Janson, A.A.M., Ginjaar, H.B., Breuning, M.H., and den Dunnen, J.T. (2006). Duplications in the DMD gene. *Hum. Mutat.* 27, 938–945.
5. Mendell, J.R., Rodino-Klapac, L.R., Sahenk, Z., Roush, K., Bird, L., Lowes, L.P., Alfano, L., Gomez, A.M., Lewis, S., Kota, J., et al. (2013). Eteplirsen for the treatment of Duchenne muscular dystrophy. *Ann. Neurol.* 74, 637–647. <https://doi.org/10.1002/ana.23982>.
6. Anwar, S., and Yokota, T. (2020). Golodirsen for Duchenne muscular dystrophy. *Drugs Today* 56, 491–504. <https://doi.org/10.1358/dot.2020.56.8.3159186>.
7. Wagner, K.R., Kuntz, N.L., Koenig, E., East, L., Upadhyay, S., Han, B., and Shieh, P.B. (2021). Safety, tolerability, and pharmacokinetics of casimersen in patients with Duchenne muscular dystrophy amenable to exon 45 skipping: A randomized, double-blind, placebo-controlled, dose-titration trial. *Muscle Nerve* 64, 285–292. <https://doi.org/10.1002/mus.27347>.
8. Clemens, P.R., Rao, V.K., Connolly, A.M., Harper, A.D., Mah, J.K., Smith, E.C., McDonald, C.M., Zaidman, C.M., Morgenroth, L.P., Osaki, H., et al. (2020). Safety, Tolerability, and Efficacy of Viltolarsen in Boys With Duchenne Muscular Dystrophy Amenable to Exon 53 Skipping: A Phase 2 Randomized Clinical Trial. *JAMA Neurol.* 77, 982–991. <https://doi.org/10.1001/jamaneurol.2020.1264>.
9. Wein, N., Vulin, A., Falzarano, M.S., Zsigyarto, C.A.K., Maiti, B., Findlay, A., Heller, K.N., Uhlén, M., Bakthavachalu, B., Messina, S., et al. (2014). Translation from a DMD exon 5 IRES results in a functional dystrophin isoform that attenuates dystrophinopathy in humans and mice. *Nat. Med.* 20, 992–1000. <https://doi.org/10.1038/nm.3628>.
10. Flanigan, K.M., Dunn, D.M., von Niederhausern, A., Howard, M.T., Mendell, J., Connolly, A., Saunders, C., Modrcin, A., Dasouki, M., Comi, G.P., et al. (2009). DMD Trp3X nonsense mutation associated with a founder effect in North American families with mild Becker muscular dystrophy. *Neuromuscul. Disord.* 19, 743–748. <https://doi.org/10.1016/j.nmd.2009.08.010>.
11. Gurvich, O.L., Maiti, B., Weiss, R.B., Aggarwal, G., Howard, M.T., and Flanigan, K.M. (2009). DMD exon 1 truncating point mutations: amelioration of phenotype by

- alternative translation initiation in exon 6. *Hum. Mutat.* 30, 633–640. <https://doi.org/10.1002/humu.20913>.
12. Simmons, T.R., Vetter, T.A., Huang, N., Vulin-Chaffiol, A., Wein, N., and Flanigan, K.M. (2021). Pre-clinical dose-escalation studies establish a therapeutic range for U7snRNA-mediated DMD exon 2 skipping. *Mol. Ther. Methods Clin. Dev.* 21, 325–340. <https://doi.org/10.1016/j.omtm.2021.03.014>.
 13. Wein, N., Dunn, D.M., Waldrop, M.A., Gushchina, L.V., Frair, E.C., Weiss, R.B., and Flanigan, K.M. (2021). Absence of Significant Off-Target Splicing Variation with a U7snRNA Vector Targeting DMD Exon 2 Duplications. *Hum. Gene Ther.* 32, 1346–1359. <https://doi.org/10.1089/hum.2020.315>.
 14. Gushchina, L.V., Frair, E.C., Rohan, N., Bradley, A.J., Simmons, T.R., Chavan, H.D., Chou, H.J., Eggers, M., Waldrop, M.A., Wein, N., and Flanigan, K.M. (2021). Lack of toxicity in non-human primates receiving clinically relevant doses of an AAV9.U7snRNA vector designed to induce DMD exon 2 skipping. *Hum. Gene Ther.* 32, 882–894. <https://doi.org/10.1089/hum.2020.286>.
 15. Wein, N., Vetter, T.A., Vulin, A., Simmons, T.R., Frair, E.C., Bradley, A.J., Gushchina, L.V., Almeida, C.F., Huang, N., Lesman, D., et al. (2022). Systemic delivery of an AAV9 exon-skipping vector significantly improves or prevents features of Duchenne muscular dystrophy in the Dup2 mouse. *Mol. Ther. Methods Clin. Dev.* 26, 279–293. <https://doi.org/10.1016/j.omtm.2022.07.005>.
 16. Vulin, A., Wein, N., Simmons, T.R., Rutherford, A.M., Findlay, A.R., Yurkoski, J.A., Kaminoh, Y., and Flanigan, K.M. (2015). The first exon duplication mouse model of Duchenne muscular dystrophy: A tool for therapeutic development. *Neuromuscul. Disord.* 25, 827–834. <https://doi.org/10.1016/j.nmd.2015.08.005>.
 17. Gushchina, L.V., Vetter, T.A., Frair, E.C., Bradley, A.J., Grounds, K.M., Lay, J.W., Huang, N., Suhaiba, A., Schnell, F.J., Hanson, G., et al. (2022). Systemic PPMO-mediated dystrophin expression in the Dup2 mouse model of Duchenne muscular dystrophy. *Mol. Ther. Nucleic Acids* 30, 479–492. <https://doi.org/10.1016/j.omtn.2022.10.025>.
 18. Zambon, A.A., Waldrop, M.A., Alles, R., Weiss, R.B., Conroy, S., Moore-Clingenpeel, M., Previtali, S., and Flanigan, K.M.; Italian DMD Network and the United Dystrophinopathy Project; the United Dystrophinopathy Project (2022). Phenotypic Spectrum of Dystrophinopathy Due to Duchenne Muscular Dystrophy Exon 2 Duplications. *Neurology* 98, e730–e738. <https://doi.org/10.1212/WNL.00000000000013246>.
 19. Nigro, G., Comi, L.L., Politano, L., and Bain, R.J. (1990). The incidence and evolution of cardiomyopathy in Duchenne muscular dystrophy. *Int. J. Cardiol.* 26, 271–277. [https://doi.org/10.1016/0167-5273\(90\)90082-g](https://doi.org/10.1016/0167-5273(90)90082-g).
 20. Malerba, A., Boldrin, L., and Dickson, G. (2011). Long-term systemic administration of unconjugated morpholino oligomers for therapeutic expression of dystrophin by exon skipping in skeletal muscle: implications for cardiac muscle integrity. *Nucleic Acid Therapeut.* 21, 293–298. <https://doi.org/10.1089/nat.2011.0306>.
 21. Potter, R.A., Griffin, D.A., Heller, K.N., Peterson, E.L., Clark, E.K., Mendell, J.R., and Rodino-Klapac, L.R. (2021). Dose-Escalation Study of Systemically Delivered rAAVrh74.MHCK7.micro-dystrophin in the mdx Mouse Model of Duchenne Muscular Dystrophy. *Hum. Gene Ther.* 32, 375–389. <https://doi.org/10.1089/hum.2019.255>.
 22. Forand, A., Muchir, A., Mougnot, N., Sevoz-Couche, C., Peccate, C., Lemaitre, M., Isabelle, C., Wood, M., Lorain, S., and Piétri-Rouxel, F. (2020). Combined Treatment with Peptide-Conjugated Phosphorodiamidate Morpholino Oligomer-PPMO and AAV-U7 Rescues the Severe DMD Phenotype in Mice. *Mol. Ther. Methods Clin. Dev.* 17, 695–708. <https://doi.org/10.1016/j.omtm.2020.03.011>.
 23. Gan, L., Wu, L.C.L., Wood, J.A., Yao, M., Treleaven, C.M., Estrella, N.L., Wentworth, B.M., Hanson, G.J., and Passini, M.A. (2022). A cell-penetrating peptide enhances delivery and efficacy of phosphorodiamidate morpholino oligomers in mdx mice. *Mol. Ther. Nucleic Acids* 30, 17–27. <https://doi.org/10.1016/j.omtn.2022.08.019>.
 24. Megan, A., Waldrop, M.W.L., Vetter, T.A., Frair, E., Beatka, M., Meng, H., Iammarino, M., Sabo, B., Subramanian, S., Kaler, M.M., et al. (2023). Presidential Symposium and Presentation of Top Abstracts. *Mol. Ther.* 31, 1–794. <https://doi.org/10.1016/j.ymthe.2023.04.017>.
 25. Liu, M., Yue, Y., Harper, S.Q., Grange, R.W., Chamberlain, J.S., and Duan, D. (2005). Adeno-associated virus-mediated microdystrophin expression protects young mdx muscle from contraction-induced injury. *Mol. Ther.* 11, 245–256. <https://doi.org/10.1016/j.ymthe.2004.09.013>.
 26. Le Guiner, C., Servais, L., Montus, M., Larcher, T., Fraysse, B., Moullec, S., Allais, M., François, V., Dutilleul, M., Malerba, A., et al. (2017). Long-term microdystrophin gene therapy is effective in a canine model of Duchenne muscular dystrophy. *Nat. Commun.* 8, 16105. <https://doi.org/10.1038/ncomms16105>.
 27. Mendell, J.R., Sahenk, Z., Lehman, K., Nease, C., Lowes, L.P., Miller, N.F., Iammarino, M.A., Alfano, L.N., Nicholl, A., Al-Zaidy, S., et al. (2020). Assessment of Systemic Delivery of rAAVrh74.MHCK7.micro-dystrophin in Children With Duchenne Muscular Dystrophy: A Nonrandomized Controlled Trial. *JAMA Neurol.* 77, 1122–1131. <https://doi.org/10.1001/jamaneurol.2020.1484>.
 28. Duan, D. (2018). Systemic AAV Micro-dystrophin Gene Therapy for Duchenne Muscular Dystrophy. *Mol. Ther.* 26, 2337–2356. <https://doi.org/10.1016/j.ymthe.2018.07.011>.
 29. Mingozzi, F., and High, K.A. (2013). Immune responses to AAV vectors: overcoming barriers to successful gene therapy. *Blood* 122, 23–36. <https://doi.org/10.1182/blood-2013-01-306647>.
 30. Ronzitti, G., Gross, D.A., and Mingozzi, F. (2020). Human Immune Responses to Adeno-Associated Virus (AAV) Vectors. *Front. Immunol.* 11, 670. <https://doi.org/10.3389/fimmu.2020.00670>.
 31. Prasad, S., Dimmock, D.P., Greenberg, B., Walia, J.S., Sadhu, C., Tavakkoli, F., and Lipshutz, G.S. (2022). Immune Responses and Immunosuppressive Strategies for Adeno-Associated Virus-Based Gene Therapy for Treatment of Central Nervous System Disorders: Current Knowledge and Approaches. *Hum. Gene Ther.* 33, 1228–1245. <https://doi.org/10.1089/hum.2022.138>.
 32. Arjomandnejad, M., Dasgupta, I., Flotte, T.R., and Keeler, A.M. (2023). Immunogenicity of Recombinant Adeno-Associated Virus (AAV) Vectors for Gene Transfer. *BioDrugs* 37, 311–329. <https://doi.org/10.1007/s40259-023-00585-7>.
 33. Srivastava, A. (2023). Rationale and strategies for the development of safe and effective optimized AAV vectors for human gene therapy. *Mol. Ther. Nucleic Acids* 32, 949–959. <https://doi.org/10.1016/j.omtn.2023.05.014>.
 34. Hakim, C.H., Grange, R.W., and Duan, D. (2011). The passive mechanical properties of the extensor digitorum longus muscle are compromised in 2- to 20-mo-old mdx mice. *J. Appl. Physiol.* 110, 1656–1663. <https://doi.org/10.1152/jappphysiol.01425.2010>.
 35. Hakim, C.H., Li, D., and Duan, D. (2011). Monitoring murine skeletal muscle function for muscle gene therapy. *Methods Mol. Biol.* 709, 75–89. https://doi.org/10.1007/978-1-61737-982-6_5.
 36. Burkholder, T.J., Fingado, B., Baron, S., and Lieber, R.L. (1994). Relationship between muscle fiber types and sizes and muscle architectural properties in the mouse hindlimb. *J. Morphol.* 221, 177–190. <https://doi.org/10.1002/jmor.1052210207>.
 37. Pozsgai, E.R., Griffin, D.A., Heller, K.N., Mendell, J.R., and Rodino-Klapac, L.R. (2017). Systemic AAV-Mediated beta-Sarcoglycan Delivery Targeting Cardiac and Skeletal Muscle Ameliorates Histological and Functional Deficits in LGMD2E Mice. *Mol. Ther.* 25, 855–869. <https://doi.org/10.1016/j.ymthe.2017.02.013>.
 38. Berry, G.E., and Tse, L.V. (2017). Virus Binding and Internalization Assay for Adeno-associated Virus. *Bio. Protoc.* 7, e2110. <https://doi.org/10.21769/BioProtoc.2110>.
 39. Vetter, T.A., Nicolau, S., Bradley, A.J., Frair, E.C., and Flanigan, K.M. (2022). Automated immunofluorescence analysis for sensitive and precise dystrophin quantification in muscle biopsies. *Neuropathol. Appl. Neurobiol.* 48, e12785. <https://doi.org/10.1111/nan.12785>.